Available online at www.sciencedirect.com
SCIENCE DIRECT®
Geochimica et Cosmochimica Acta 70 (2006) 1457–1470
Geochimica
www.elsevier.com/locate/gca

Stable isotope and Rare Earth Element evidence for recent ironstone pods within the Archean Barberton greenstone belt, South Africa

Michael T. Hren [a,*], Donald R. Lowe [a], Michael M. Tice [a,1], Gary Byerly [b], C. Page Chamberlain [a]

[a] Department of Geological and Environmental Sciences, Stanford University, Building 320, Lomita Mall, Stanford, CA 94305, USA
[b] Department of Geology and Geophysics, Louisiana State University, Baton Rouge, LA 70803-4101, USA

Received 5 July 2005; accepted in revised form 17 November 2005

Abstract

There is considerable debate about the mode and age of formation of large (up to ~200 m long) hematite and goethite ironstone bodies within the 3.2 to 3.5 Ga Barberton greenstone belt. We examined oxygen and hydrogen isotopes and Rare Earth Element (REE) concentrations of goethite and hematite components of the ironstones to determine whether these deposits reflect formation from sea-floor vents in the Archean ocean or from recent surface and shallow subsurface spring systems. Goethite $\delta^{18}O$ values range from −0.7 to +1.0‰ and δD from −125 to −146‰, which is consistent with formation from modern meteoric waters at 20 to 25 °C. Hematite $\delta^{18}O$ values range from −0.7 to −2.0‰, which is consistent with formation at low to moderate temperatures (40–55 °C) from modern meteoric water. REE in the goethite and hematite are derived from the weathering of local sideritic ironstones, silicified ultramafic rocks, sideritic black cherts, and local felsic volcanic rocks, falling along a mixing line between the Eu/Eu* and shale-normalized $HREE_{Avg}/LREE_{Avg}$ values for the associated silicified ultramafic rocks and felsic volcanic rocks. Contrasting positive Ce/Ce* of 1.3 to 3.5 in hematite and negative Ce/Ce* of 0.2 to 0.9 in goethite provides evidence of oxidative scavenging of Ce on hematite surfaces during mineral precipitation. These isotopic and REE data, taken together, suggest that hematite and goethite ironstone pods formed from relatively recent meteoric waters in shallow springs and/or subsurface warm springs.

1. Introduction

Chemical sediments preserved in Archean rocks provide a valuable geochemical record of the conditions on the surface of the early Earth. Many of these Archean chemical sediments contain a high percentage of oxidized iron, frequently found in discrete alternating iron and silica-rich bands or lenses, and commonly identified as banded iron formations (BIFs). These iron-rich units are generally interpreted to have formed in marine basins where mixing of slightly oxidizing solutions with waters rich in reduced iron results in rapid precipitation and accumulation of iron oxyhydroxides (Drever, 1974; Kasting, 1987; Danielson et al., 1992). Because many of these deposits are interpreted to have formed directly in the marine environment, the geochemical record provided by these sediments has been used to infer paleo-ocean temperatures, depth, redox potential, chemical stratification, and the rise of oxygen in the atmosphere (Fryer, 1977; Derry and Jacobsen, 1990; Towe, 1991; Danielson et al., 1992; Alibert and McCulloch, 1993; de Ronde et al., 1994; Channer et al., 1997; de Ronde et al., 1997;

* Corresponding author. Fax: +1 650 725 2199.
E-mail address: hren@stanford.edu (M.T. Hren).
[1] Present address: Department of Geological and Planetary Sciences, Caltech, Pasadena, CA 91125, USA.

0016-7037/$ - see front matter © 2005 Elsevier Inc. All rights reserved.
doi:10.1016/j.gca.2005.11.016

Kato et al., 1998; Bau and Dulski, 1999; Harrison, 1999; Bjerrum and Canfield, 2002; Bolhar et al., 2004). Some iron-rich formations within Archean units contain structural features suggestive of relict marine hydrothermal vent structures (de Wit et al., 1982; de Ronde et al., 1994). Specifically, large hematite- and goethite-rich bodies identified by de Wit et al. (1982) and de Ronde et al. (1994) which rest on the Onverwacht and Fig Tree Groups of the 3.2–3.5 Ga Barberton greenstone belt, have been interpreted to be remnants of hydrothermal vent systems formed on the Archean sea-floor (de Wit et al., 1982; de Ronde et al., 1994). These ironstone deposits have yielded potentially the oldest complex organic molecules identified to date, and have been interpreted to show microbial communities populating Archean vent systems at least 3.2 Ga (de Ronde and Ebbesen, 1996). However, recent examination of some ironstone pods suggests that the ironstones found across portions of the southern part of the Barberton belt are not marine hydrothermal vent structures, but rather chemical precipitates formed in recent shallow spring or low temperature hydrothermal systems (Lowe and Byerly, 2003).

BIFs and ironstones formed in the deep ocean during the Archean period may provide one of the few well-preserved records of chemical conditions on the Early Earth including the hydrothermal/continental flux to the oceans, redox state of the ocean, and organic composition of early life on Earth. In light of the controversy regarding the mode of formation for the ironstone pods in the 3.2–3.5 Ga Barberton greenstone belt, a potentially valuable geochemical proxy for conditions in the Archean ocean, it is critical that we are able to distinguish true Archean deposits from recent chemical precipitates replacing original ancient units. We present here a combined stable isotope and Rare Earth Element (REE) data set that suggests that the ironstone pods on Farm Mendon, Barberton, South Africa formed as a result of recent remobilization of iron from local Archean sideritic ironstones, siderite-bearing chert units, ultramafic rocks, and felsic volcanics, and precipitation from surface and shallow subsurface waters and/or warm springs.

2. Geologic setting and ironstone pods

The Barberton greenstone belt contains some of the best-preserved sequences of Archean marine and continentally derived sediments. The stratigraphic succession containing the ironstone pods within the Barberton greenstone belt (3.2–3.5 Ga) consists of a predominantly volcanic sequence (Onverwacht Group) overlain by the dominantly sedimentary Fig Tree and Moodies groups (de Wit et al., 1982; Lowe and Byerly, 1999). The classic ironstone pods of de Ronde et al. (1994) on Farm Mendon are associated with structurally complex outcrops of silicified and serpentinized ultramafic volcanic rocks of the Mendon Formation (Onverwacht Group) capping black cherts and overlying BIFs, felsic pyroclastic deposits, and interbedded clastic rocks of the Fig Tree Group (Lowe and Byerly, 1999, 2003). Archean felsic porphyry locally intrudes ultramafic rocks of the Mendon Formation (de Wit et al., 1982) but not the ironstone pods (Lowe and Byerly, 2003).

The ironstone pods occur as irregular, lense-shaped bodies up to 200 m long and 60 m across in three major localities along 15 km of strike in the south central portion of the greenstone belt (de Wit et al., 1982; Lowe and Byerly, 1999, 2003). They are composed primarily of dark brown goethite (FeO(OH)), but the largest pod of the group on Farm Mendon is composed mainly of hematite (Fe_2O_3). All show irregular, rotated chunks and masses of coarsely crystalline cavity-fill quartz showing replacement by iron oxides.

Iron oxides were sampled from three ironstone pod localities originally described by de Wit et al. (1982) and more recently by Lowe and Byerly (1999, 2003) on Farm Mendon within the Barberton greenstone belt of South Africa (location map, Fig. 1). The samples analyzed in this work represent surface and near-surface exposures of hematite and goethite from an abandoned mine in the central hematite pod on Farm Mendon (25°54.395′S, 31°01.367′E; samples SA574-1 to 6 and SAF495-6) (Fig. 1), surface exposures of goethite boxwork exposed in low road cuts through the easternmost pod (25°54.383′S, 31°01.455′E; SAF495-10 and SAF495-3), and goethite from the surface of the westernmost pod (25°54.377′S, 31°01.077′E; SAF495-1, SAF495-4, and SAF495-7). In addition, goethite was analyzed from an inactive modern surface spring deposit on Farm Avontuur (25°55.749′S, 30°50.178′E; SAF492-18), described by Lowe and Byerly (2003).

3. Analytical methods

3.1. Sample preparation and characterization

Goethite and hematite samples collected from the ironstone pods were reduced to coarse (2–4 cm) chips with a rock hammer and cut with a water-cooled rock saw to expose fresh surfaces and avoid chemical effects possibly associated with weathered rinds. Goethite and hematite powders were drilled from freshly cut surfaces using a fine-tipped diamond dental drill. Drilled powders were sieved to <63 μm prior to chemical treatment. Fine-grained powders were heated to ~100 °C in 5 M NaOH solution for 3 h and washed in 0.5 M HCl for 20 min at room temperature to remove amorphous iron oxyhydroxides, gibbsite, kaolinite, 2:1 phylosilicates, calcite, and siderite (Kämpf and Schwertmann, 1982; Yapp, 1991). Following chemical treatment, samples were rinsed with de-ionized water 4–5 times and dried in a vacuum oven for 24 h at room temperature and at 80 °C for 1 h before X-ray diffraction and isotope analyses.

X-ray diffraction patterns of both goethite and hematite showed minimal or no change upon chemical treat-

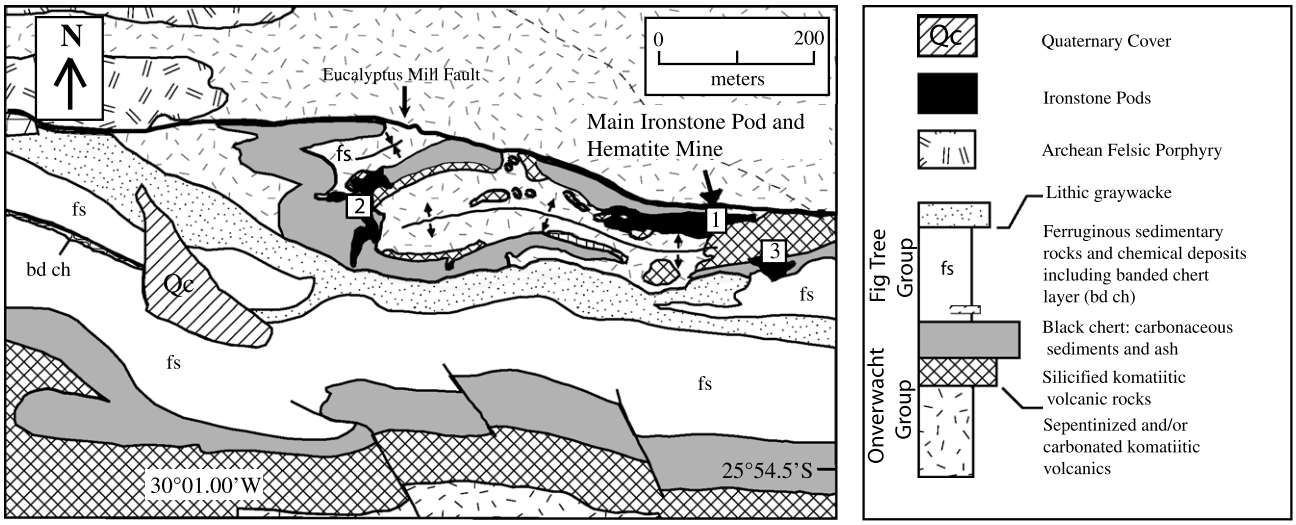

Fig. 1. Geologic map of ironstone pods on Farm Mendon, Barberton greenstone belt (modified from Lowe and Byerly, 2003). Hematite samples collected from an abandoned mine in the central pod (1). Surface goethites collected from the western pod (2) and the eastern pod (3).

ment. In addition, oxygen and hydrogen isotope analyses of several untreated samples that displayed the best X-ray diffraction patterns and were likely to be the least contaminated (purest goethite and/or hematite), showed little (<0.5‰ for $\delta^{18}O$ and <6‰ for δD) to no isotopic difference between treated and untreated samples (Table 1). These results suggest that chemical treatments resulted in minimal goethite recrystallization or isotopic exchange with chemical solutions. The lack of isotopic exchange confirms the results of other studies, that this chemical treatment does not affect the isotopic composition of iron oxyhydroxides (Yapp, 1991; Poage et al., 2000; Sjostrom et al., 2004).

Powdered mineral separates were mounted in glass holders and analyzed by X-ray diffraction. Diffraction patterns of hematite and goethite revealed nearly "pure" mineral separates (Figs. 2 and 3). One hematite sample and several of the goethite samples display a weakly developed quartz peak, indicating possible contamination induced by drilling a portion of the minor quartz veins associated with some oxide samples. However, diffraction patterns show that if there were contamination by quartz, it is only at most a few percent and, as such, will not significantly affect the isotopic or chemical analyses of these samples. We also used an ammonium oxalate treatment (Jackson et al., 1982) to determine the amount of amorphous or poorly crystalline iron oxide phases, as these may not be detectable in X-ray diffraction. Dissolved iron concentrations were measured at Stanford University using an inductively coupled plasma spectrometer (ICP). All samples show less than 1.5% of dissolvable iron oxide phases (Table 1), confirming our assessment that all samples are nearly pure goethite or hematite.

Goethite and hematite samples were analyzed for Si, Al, and Mn on a JEOL JXA-733A electron microprobe at Stanford University. Multiple spot analyses of each sample show that all goethite samples have less than 2.5 weight% SiO_2 and less than 0.8 weight percent Al_2O_3. Hematite samples all have less than 1 weight% SiO_2 and less than 0.4 weight percent Al_2O_3. No samples showed a detectable amount of Mn in the mineral matrix.

3.2. Isotope and chemical analyses

Ten to twenty milligrams goethite or hematite powder were weighed and dried in a vacuum oven at 80 °C for 1 h. Samples were placed in a dry box in a nitrogen atmosphere and loaded into nickel reaction vessels. Samples were outgassed in reaction vessels under vacuum for 1 h at 100 °C and 2 h at room temperature prior to reaction. Oxygen isotope analyses were conducted using fluorination techniques following the method of Clayton and Mayeda (1963), using BrF_5 as the oxidizing agent to liberate oxygen gas from the goethite and hematite powders, and analyzed on a Finnigan Delta Plus XL. All isotopic analyses of oxygen and hydrogen are reported in standard δ-notation, which is defined as:

$$\delta^{*}Y = \left(\frac{R_{\text{sample}} - R_{\text{std}}}{R_{\text{std}}}\right) \times 1000,$$

where R is the ratio of heavy to light isotopes in the sample and in the standard and $^{*}Y$ is the isotope that appears in the numerator of R. Delta values are reported relative to V-SMOW (Vienna Standard Mean Ocean Water). Repeat analyses of NBS-28 (quartz) and FCol-3 (goethite), a laboratory standard provided by Dr. Crayton Yapp, yield a precision of ±0.3‰.

Hydrogen isotopes were analyzed in a Temperature Conversion Elemental Analyzer (TC/EA) following the method of Sharp et al. (2001). Approximately 0.6–1.0 mg of treated goethite powder was loaded in a silver crucible. Weighed samples were placed in a vacuum oven at 80 °C

Table 1
Oxygen and hydrogen isotope data for treated and untreated samples and weight% contaminants for goethite and hematite samples

Goethite	Untreated sample		Treated sample		Weight % SiO_2	Weight% $A1_2O_3$	Weight % oxalate extractable	Calculated temperature of formation (°C)[a]	Source
	$\delta^{18}O_{goethite}$	$\delta D_{goethite}$	$\delta^{18}O_{goethite}$	$\delta D_{goethite}$					
SAF495-1	1.3	−127	0.6	−129	1.2	0.1	0.28	21	50 cm deep goethite mound, western pod
SAF495-3	1.2	−122	1.0	−127	1.8	0.8	1.45	20	Exposed vein in chert, eastern pod
SAF495-4	2.6	−115	0.9	−125	2.0	0.1	0.04	23	Surface spring deposit
SAF495-6	1.3	−140	1.0	−146	1.1	0.5	0.32	1	Surface, central pod, mine
SAF495-7	−0.2	−130	−0.7	−135	1.5	0.1	0.39	25	Surface sample, western pod
SAF495-10	−0.2	−127	0.2	−130	2.5	0.1	0.38	23	Surface exposed boxwork, eastern pod
SAF492-18	1.0	−116	0.5	−127	1.1	0.1	0.04	24	Surface terrace, lower pod

Hematite	Untreated sample $\delta^{18}O_{hematite}$	Treated sample $\delta^{18}O_{hematite}$	Weight% SiO_2	Weight% Al_2O_3	Weight% oxalate extractable	Calculated temperature of formation in eq. with meteoric waters (°C)[b]	Calculated temperature of formation in eq. with Archean ocean (°C)[c]	Source
SA574-1.	—	−1.0	1.0	0.4	0.60	44	90	Subsurface, mine, central pod
SA574-2	—	−2.0	0.1	0.2	0.71	54	107	Subsurface, mine, central pod
SA574-3	−1.1	−1.6	0.5	0.2	0.74	50	100	Subsurface, mine, central pod
SA574-4	−1.3	−1.5	0.3	0.2	0.07	49	99	Subsurface, mine, central pod
SA574-5	—	−0.7	0.1	0.1	0.16	41	87	Subsurface, mine, central pod

[a] $^{D}\alpha_{goethite-water}$ and $^{18}\alpha_{goethite-water}$ from Yapp (1987, 2001).
[b] $^{18}\alpha_{hematite-water}$ from Yapp (1990a, 2001). $\delta^{18}O_{water} = -5‰$.
[c] $^{18}\alpha_{hematite-water}$ from Yapp (1990a, 2001). (Using an Archaean ocean $\delta^{18}O$ of $-1‰$).

for 1 h to remove adsorbed water, then rapidly transferred to a sealed autosampler and flushed with dry helium at room temperature for 2 h. Samples were then reacted in the TC/EA at 1450 °C, producing H_2 gas, which was then carried in a stream of helium and analyzed using a Finnigan Delta Plus XL. Repeat analyses of NIST standards NBS-22 (hydrocarbon oil), PEF-1 (polyethylene foil), and FCol-3 (goethite) yield a precision of ±3.0‰.

To test whether there was significant isotopic heterogeneity in our goethite and hematite samples we measured hydrogen and oxygen isotope values of subsamples taken from within different portions of a single rock sample. We found that δD and $\delta^{18}O$ values varied by less than 6‰ and 0.5‰, respectively, within a single hand sample.

Rock chips were prepared and analyzed for a suite of 27 trace elements at Washington State University Geoanalytical laboratory. Approximately 250 mg of powdered sample was dissolved at 110 °C, using 2 mL concentrated HCl, 6 mL HF, 2 mL HNO_3, and 2 mL $HClO_4$ in an open Teflon vial. Samples were then evaporated to dryness, followed by additional evaporation with 2 mL $HClO_4$ at 165 °C. Three milliliters HNO_3, 8 drops H_2O_2, and 5 drops HF, and internal standards of In, Re, and Ru were added to the sample and diluted to a final volume of 60 mL. Digested samples were analyzed on a Sciex Elan model 250 ICP-MS. Accuracy of these analyses is approximately 5%.

4. Results

4.1. Oxygen and hydrogen isotopes of goethite and hematite

We determined both the oxygen and hydrogen isotope composition of goethite. $\delta^{18}O$ values of goethite samples range from −0.7‰ to 1.0‰, with a mean $\delta^{18}O$ value of 0.5‰ ± 0.6 (1σ). δD values of goethite range from −125‰ to −146‰ with the mean δD of these samples of −131‰ ± 7 (1σ). $\delta^{18}O$ and δD values of goethite co-vary linearly ($R^2 = 0.89$) with a slope slightly lower than that of the Global Meteoric Water Line (GMWL, Fig. 4).

We also measured the oxygen isotope composition of hematite. These hematite samples have $\delta^{18}O$ values ranging from −2.0‰ to −0.7‰ (Table 1). The mean $\delta^{18}O$ value of these samples is −1.4‰ ± 0.5 (1σ). The oxygen isotope val-

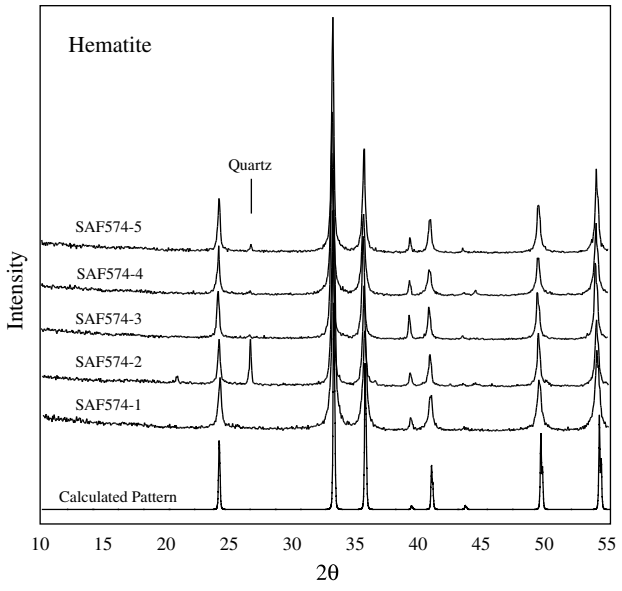

Fig. 2. XRD pattern for treated hematite samples from the central pod. Included is a calculated diffraction pattern for a pure hematite. Hematite XRD patterns show minimal contamination by other mineral species (quartz) that is at most only a few percent and does not significantly affect geochemical analyses.

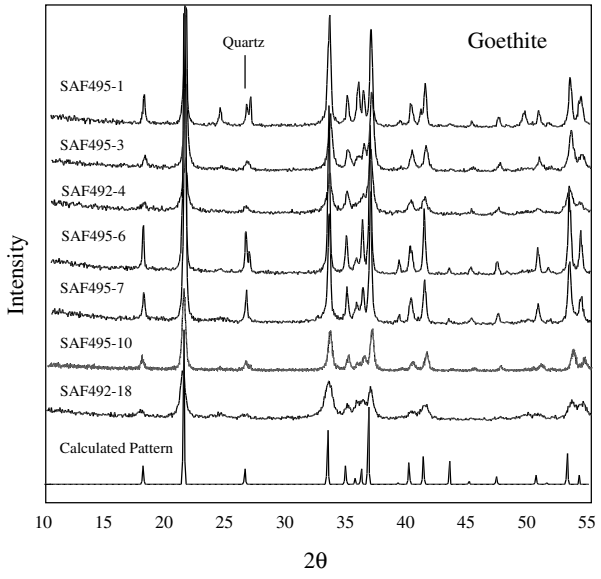

Fig. 3. XRD pattern for treated goethite samples from surface exposures of all three ironstone pods. Diffraction patterns show minor contamination by other mineral species (quartz) which is not expected to significantly effect geochemical analyses.

ues reported here are consistent with previous analyses of similar hematite and goethite samples from the ironstone pods (de Ronde et al., 1994), which showed a range of 0.7‰ to −3.1‰ (excluding one outlier at −6.7‰).

4.2. REE distribution in hematite and goethite

Hematite, goethite, and a suite of associated Archean igneous and sedimentary units were analyzed for REE concentrations (Table 2). All REE concentrations reported here are normalized to the Post Archean Australian Shale (PAAS) (Taylor and McLellan, 1985). These data show distinctive Rare Earth Element (REE) patterns, and Ce and Eu anomalies (Fig. 5). The majority of the hematite samples that we examined show a slight shale-normalized HREE enrichment, which is consistent with REE patterns in associated Archean black cherts and ultramafic and felsic rocks (Figs. 7 and 8). These shale-normalized, HREE-enriched hematite samples also show positive Ce and Eu anomalies (Fig. 5; Table 2). Following McLennon (1989), positive Ce and Eu anomalies are defined by shale normalized Ce/Ce* and Eu/Eu* values greater than 1, where $Ce/Ce^* = Ce_{SN}/(La_{SN}{*}Pr_{SN})^{0.5}$ and $Eu/Eu^* = Eu_{SN}/(Sm_{SN}{*}Gd_{SN})^{0.5}$. Hematite samples show a range of positive Ce/Ce*, from 1.2 to 3.2 and positive Eu/Eu*, from 1.6 to 2.4. The two samples which do not display the HREE enrichment fail to show anomalous Ce, although they do have positive Eu anomalies (Fig. 5; Table 2).

Like hematite, the majority of goethite samples also show shale-normalized enrichment of HREEs, and an overall REE enrichment relative to hematite. These also have positive Eu anomalies (Eu/Eu* = 1.3–1.8) (Fig. 6; Table 2). Unlike hematite however, most goethites display no or negative Ce anomalies, with Ce/Ce* values ranging from 0.2 to 1.1. One sample (SAF492-18), however, has a strong positive Ce anomaly (Ce/Ce* = 9.9), which may be due to an inclusion of a Ce-rich mineral within the goethite. Three of the goethite samples, SAF495-1, SAF494-3, and SAF495-4, bear strong similarities to the REE patterns observed in locally associated silicified ultramafic rocks (Figs. 6 and 8). The REE patterns of the remaining goethites bear a greater resemblance to associated sedimentary (sideritic ironstone and black cherts) and felsic volcanic units (Fig. 7).

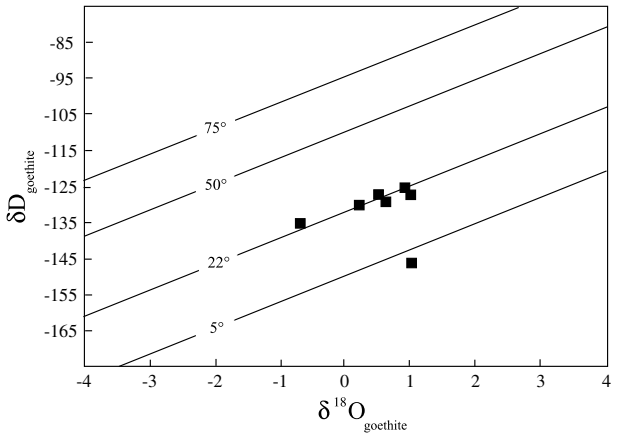

Fig. 4. Using the equations outlined in Yapp (2001) it is possible to generate a set of isotherms representing the temperature of formation of goethites with a range of measured oxygen and hydrogen isotope compositions. A plot of the measured δD versus the $\delta^{18}O$ of goethites from the ironstone pods shows that samples plot in an array along the calculated 22 °C line. The range of temperatures of formation for the goethites sampled are in good agreement with the mean annual temperature of the Barberton region (20–22 °C) with the exception of one outlier which falls below the 5 °C isotherm.

Table 2
Elemental concentrations (ppm)

	Hematite						Goethite						
	SA574-1	SA574-2	SA574-3	SA574-4	SA574-5	SA574-6	SAF495-1	SAF494-3	SAF492-4	SAF495-6	SAF495-7	SAF495S-10	SAF492-18
La	0.47	0.13	1.79	0.22	0.38	4.86	3.65	3.17	5.44	0.80	2.28	3.79	6.65
Ce	2.86	1.26	3.16	0.57	0.72	6.82	8.85	9.35	132.39	1.71	4.14	1.06	7.45
Pr	0.18	0.05	0.28	0.05	0.07	0.62	0.91	1.60	1.73	0.20	0.55	0.40	1.55
Nd	0.78	0.15	1.04	0.16	0.27	2.22	3.52	7.82	7.97	0.84	2.39	1.62	8.29
Sm	0.33	0.05	0.23	0.05	0.07	0.52	0.77	2.54	2.44	0.21	0.64	0.32	3.53
Eu	0.15	0.03	0.06	0.02	0.02	0.16	0.20	0.87	1.07	0.06	0.22	0.09	2.24
Gd	0.45	0.06	0.20	0.06	0.07	0.50	0.54	2.50	3.31	0.20	0.64	0.32	8.06
Tb	0.09	0.01	0.03	0.01	0.01	0.07	0.07	0.43	0.56	0.03	0.10	0.05	1.60
Dy	0.51	0.04	0.18	0.07	0.08	0.34	0.36	2.69	3.57	0.14	0.56	0.26	11.75
Ho	0.09	0.01	0.03	0.01	0.02	0.06	0.07	0.55	0.74	0.03	0.12	0.05	2.68
Er	0.21	0.02	0.08	0.03	0.05	0.13	0.22	1.52	1.98	0.09	0.31	0.15	7.24
Tm	0.03	0.00	0.01	0.01	0.01	0.02	0.03	0.24	0.27	0.01	0.05	0.02	0.98
Yb	0.15	0.02	0.07	0.03	0.05	0.10	0.25	1.63	1.64	0.10	0.31	0.12	6.07
Lu	0.02	0.00	0.01	0.01	0.01	0.01	0.04	0.27	0.26	0.02	0.05	0.02	0.93
Ba	29	5	12	8	4	11	6	3	16	2	5	1	25
Th	0.04	0.06	0.02	0.01	0.17	0.06	0.64	0.08	0.11	0.09	0.84	0.01	0.05
Nb	0.36	0.08	0.15	0.05	0.32	0.05	0.72	0.10	0.11	0.29	0.59	0.16	0.44
Y	3.39	1.70	1.23	1.89	1.51	1.58	2.38	12.91	29.02	1.25	3.70	2.92	96.40
Hf	0.12	0.11	0.03	0.11	0.13	0.05	0.23	0.04	0.04	0.05	0.32	0.02	0.04
Ta	0.00	0.03	0.00	0.00	0.02	0.01	0.02	0.00	0.00	0.00	0.07	0.00	0.01
U	2.79	0.09	0.25	0.77	0.41	1.41	0.27	0.35	1.54	0.06	0.29	0.15	1.41
Pb	2.27	1.36	1.02	1.53	0.89	2.24	1.47	1.99	2.06	0.54	1.47	0.68	98.68
Rb	0.52	0.24	0.34	0.20	0.07	0.21	0.54	0.10	0.24	0.03	0.61	0.04	0.10
Cs	0.20	0.05	0.05	0.06	0.03	0.11	0.03	0.05	0.11	0.00	0.03	0.00	0.01
Sr	5	2	2	1	1	2	3	1	2	0	9	0	5
Sc	4.9	1.7	1.5	0.8	1.1	1.9	7.0	7.9	20.8	1.9	3.8	3.0	23.7
Zr	7	6	1	6	6	3	9	1	1	2	12	1	2
Ce/Ce*	2.19	3.43	1.01	1.33	1.01	0.87	1.12	0.89	9.85	0.99	0.85	0.18	0.54
Eu/Eu*	1.8	2.4	1.3	1.7	1.4	1.5	1.5	1.6	1.7	1.4	1.6	1.3	1.8
$HREE_{Avg}/LREE_{Avg}$	2.8	1.4	0.9	2.0	1.8	0.7	0.8	2.4	2.7	1.3	1.5	0.9	7.4

Table 2 (*continued*)

	Black chert			Chert/sandstone	Felsic tuff	Sideritic ironstone	Ultramafics and silicified ultramafics				
	SAF495-37	SAF516-1	SAF517-1	SAF172-2	SAF170- 2	SAF17-K	SAF170-3	SAF181-1	SAF495-33	SAF276-1	SAF495-32
La	0.04	0.44	1.25	7.72	59.35	15.60	0.11	5.79	1.20	0.75	1.92
Ce	0.07	0.77	2.22	11.51	78.36	29.81	0.24	4.33	1.76	1.86	4.36
Pr	0.01	0.08	0.25	1.38	11.42	3.32	0.03	0.82	0.21	0.27	0.75
Nd	0.03	0.32	1.07	5.36	40.45	13.35	0.16	4.47	0.98	1.38	3.81
Sm	0.01	0.09	0.32	1.31	7.63	3.25	0.14	1.68	0.29	0.53	1.47
Eu	0.01	0.02	0.08	0.39	1.83	1.05	0.08	0.64	0.13	0.27	0.61
Gd	0.01	0.08	0.32	1.38	6.72	3.24	0.30	2.62	0.38	0.72	1.74
Tb	0.00	0.01	0.04	0.25	0.95	0.54	0.04	0.44	0.08	0.14	0.33
Dy	0.02	0.08	0.24	1.66	5.02	3.35	0.19	2.71	0.56	0.90	2.04
Ho	0.00	0.02	0.05	0.35	0.89	0.72	0.03	0.53	0.14	0.19	0.40
Er	0.01	0.05	0.13	0.97	2.02	2.00	0.08	1.19	0.38	0.51	1.05
Tm	0.00	0.01	0.02	0.15	0.27	0.30	0.01	0.13	0.06	0.07	0.15
Yb	0.01	0.05	0.11	0.92	1.60	1.83	0.07	0.69	0.35	0.43	0.87
Lu	0.00	0.01	0.02	0.15	0.24	0.29	0.01	0.09	0.05	0.07	0.14
Ba	77	2505	294	1081	1390	811	7	116	25	11	49
Th	0.02	0.17	0.36	2.61	5.38	4.86	0.05	0.19	0.06	0.08	0.13
Nb	0.03	0.28	0.43	3.21	8.70	6.64	0.17	1.42	0.41	0.55	1.04
Y	0.11	0.47	1.27	9.61	23.86	18.49	0.80	27.16	4.60	4.79	9.40
Hf	0.03	0.11	0.22	1.52	3.69	2.52	0.07	1.28	0.34	0.37	0.73
Ta	0.00	0.02	0.05	0.29	0.77	0.60	0.01	0.10	0.03	0.04	0.07
U	0.05	0.30	0.13	0.68	1.41	1.08	0.01	0.03	0.03	0.02	0.35
Pb	0.24	4.27	0.23	1.51	5.40	3.59	0.13	0.44	0.25	0.46	1.54
Rb	0.58	1.52	6.30	40.28	152.59	266.21	0.73	146.67	1.09	4.94	0.60
Cs	0.08	0.20	0.53	0.84	4.74	14.90	0.08	2.03	0.07	11.88	0.24
Sr	6	13	6	3	11	16	2	7	1	28	3
Sc	0.1	0.4	1.1	12.0	20.4	18.1	6.6	96.6	8.3	15.1	28.5
Zr	1	4	7	55	128	88	2	45	12	13	27
Ce/Ce*	0.9	0.9	0.9	0.8	0.7	1.0	1.0	0.5	0.8	0.9	0.8
Eu/Eu*	4.4	1.1	1.2	1.4	1.2	1.5	2.0	1.4	1.8	2.1	1.8
$HREE_{Avg}/LREE_{Avg}$	3.9	1.5	1.3	1.8	0.7	1.6	4.2	2.5	3.5	3.7	2.9

5. Discussion

5.1. $\delta^{18}O$ and δD in goethite and $\delta^{18}O$ of hematite as a proxy for temperature of formation and isotopic composition of waters

Because iron deposits are found over a wide range of environments and have been shown to persist over millions of years with minimal or no isotopic exchange (Yapp, 1993, 1998), numerous studies have used the oxygen, and to a lesser extent, the hydrogen isotope composition of iron oxides (hematite—$\delta^{18}O$ only; and goethite—$\delta^{18}O$ and δD) to interpret paleoenvironmental conditions of formation (Yapp and Pedley, 1985; Yapp, 1987, 1993, 1997, 2000; Girard et al., 1997; Bao and Koch, 2000; Poage et al., 2000; Girard et al., 2002; Sjostrom et al., 2004). Although there are relatively few isotopic data for iron oxides from Archean and Proterozoic rocks, several have used stable isotopes of iron oxides to constrain depositional environment, temperature range, and $\delta^{18}O$ value of water in equilibrium with

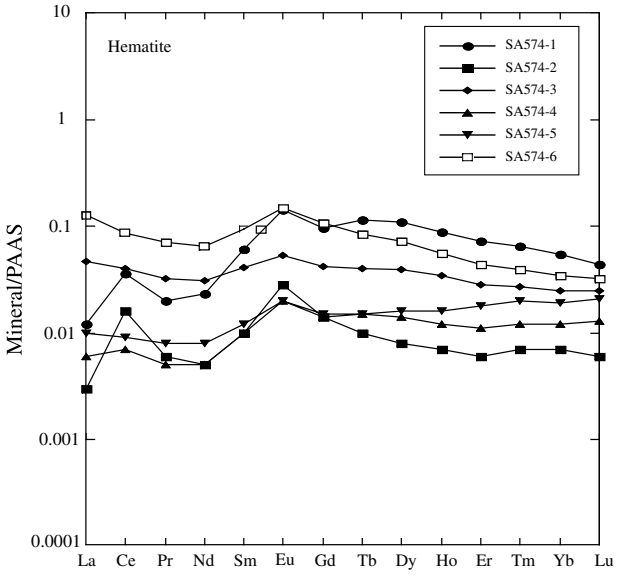

Fig. 5. Plot of the Rare Earth Element (REE) composition of hematites normalized to the Post Archean Australian Shale (PAAS). Hematite REE patterns show a range of Ce/Ce* from 0.9 to 3.4 and Eu/Eu* from 1.3 to 2.4.

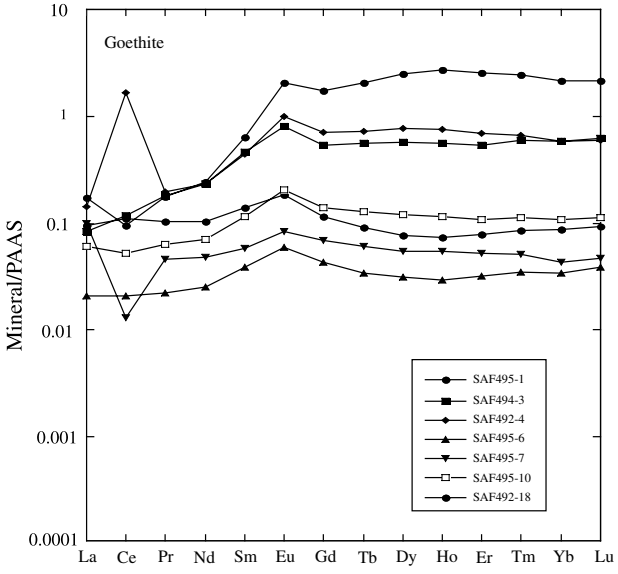

Fig. 6. Plot of Rare Earth Element (REE) composition of goethites normalized to the Post Archean Australian Shale (PAAS). Goethite REE patterns show a range of Ce/Ce* from 1.1 to 0.2 with the exception of one sample which shows strong Ce enrichment and a Ce/Ce* of 9.9. Eu/Eu* values range from 1.3 to 1.8.

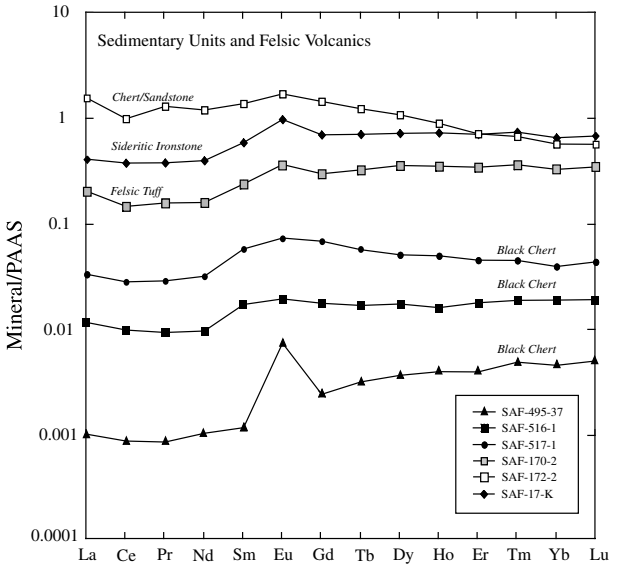

Fig. 7. Plot of the Rare Earth Element (REE) composition of associated sedimentary and felsic volcanic units. These units show no Ce enrichment and generally low Eu/Eu* values from 1.1 to 1.5. One black chert stands in sharp contrast with a strong positive Eu/Eu* enrichment of 4.4.

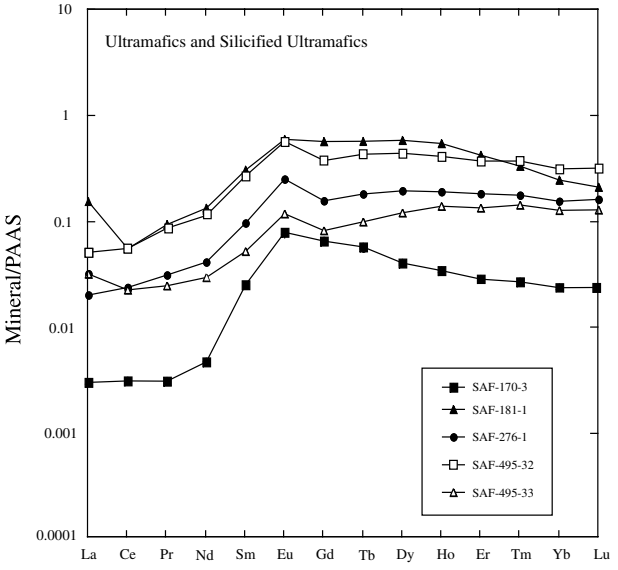

Fig. 8. Plot of the Rare Earth Element (REE) composition of associated ultramafic and silicified ultramafic rocks. These units show significant HREE enrichment and a range of Eu/Eu* values from 1.4 to 2.0.

chemically precipitated minerals (Perry et al., 1973; Perry and Ahmad, 1983; Becker and Clayton, 1976; Hoefs et al., 1987; de Ronde et al., 1994). One of these (de Ronde et al., 1994) examined the oxygen isotopes of iron oxides (both hematite and goethite) and quartz veins from the ironstone pods at Barberton and concluded that these iron oxides formed from Archean hydrothermal vents in disequilibrium with surrounding waters. However, based on combined oxygen and hydrogen isotope analyses of the iron oxides, we show that these iron oxides formed from modern surface waters and the weathering of local bedrock.

All of the arguments concerning conditions of formation require that hematite and goethite retain their original isotopic composition upon formation and do not undergo later isotopic exchange. Some iron oxide precipitates such as ferric oxide gels and poorly ordered ferrihydrite may isotopically exchange with ambient water during dissolution–reprecipitation transformations to goethite and hematite (Bao and Koch, 1999). As a result, the isotopic composition of some crystalline ferric oxides may reflect a long-term average isotopic composition of local water. However, numerous studies show that once crystallized, goethite and hematite may retain oxygen isotope values over thousands (Yapp, 1987, 1997, 2000; Girard et al., 1997, 2000, 2002; Poage et al., 2000; Sjostrom et al., 2004) to hundreds of millions of years (Yapp, 1990b, 1991, 1993, 1998; Hein et al., 1994). Likewise, it has been shown that the hydrogen isotope values of goethite do not exchange over thousands (Yapp, 1987; Poage et al., 2000; Sjostrom et al., 2004) to millions of years (Yapp and Pedley, 1985; Yapp, 1987; Girard et al., 2000). We, therefore, assume minimal or no isotopic exchange between oxides and post-depositional fluids and operate under the assumption that isotope values of goethite and hematite reflect an average isotopic composition of ambient waters at the time of formation.

The calculation of temperatures of formation of goethite is based on the methods and equations defined by Yapp (1987, 1990a, 2001). This calculation is possible because the magnitude of the fractionation of ^{18}O between goethite/hematite and water is temperature dependent, while the fractionation of deuterium between goethite and water is independent of temperature. The method to calculate temperature of formation described here follows that of Yapp (2001) and involves the following steps: First, using the temperature independent fractionation factor for hydrogen ($^{D}\alpha$), it is possible to calculate the hydrogen isotope composition of ambient waters. Second, barring significant evaporative effects, from the calculated hydrogen isotope composition of water it is possible to calculate the oxygen isotope composition of water, using the well-established equation that relates hydrogen and oxygen isotopes of meteoric water where, $\delta D = 8\delta^{18}O + 10$ (Craig, 1961; Dansgaard, 1964; Rozanski et al., 1993). Third, because the fractionation of oxygen between goethite and water is dependent upon temperature, it is possible to calculate the temperature of formation based on the measured $\delta^{18}O$ of goethite and the calculated $\delta^{18}O$ of water.

Thus, by using both $\delta^{18}O$ and δD values of goethite it is possible to determine both the temperature and isotopic composition of source water from which goethite formed (Yapp, 2001). The equations relating oxygen and hydrogen isotopes of goethite are

$$\delta D_{\text{mineral}} = 8\left(\frac{^{D}\alpha}{^{18}\alpha}\right)\delta^{18}O_{\text{mineral}} + 1000\left[8\left(\frac{^{D}\alpha}{^{18}\alpha}\right) - 1\right] - 6990\,^{D}\alpha \quad \text{(Yapp, 1987, 2000)}, \tag{1}$$

where mineral-water fractionation factors are defined by

$$^{D}\alpha_{G-W} = \frac{(D/H)_{\text{goethite}}}{(D/H)_{\text{water}}} = 0.905, \tag{2}$$

$$^{18}\alpha_{G-W} = \frac{(^{18}O/^{16}O)_{\text{goethite}}}{(^{18}O/^{16}O)_{\text{water}}} = f(\text{temperature}) \quad \text{(Yapp, 1990a)}. \tag{3}$$

The goethite–water hydrogen fractionation factor ($^{D}\alpha$) is ~0.905 Eq. (2), shows minimal variation over a temperature range of 25–145 °C (Yapp and Pedley, 1985; Yapp, 1987), and applies to goethite formed in a range of natural environments (Yapp, 1987, 1997, 2000, 2001; Girard et al., 2000). Several studies have examined the effect of temperature on the fractionation of oxygen isotopes between goethite and waters of formation (Yapp, 1987, 1990a; Zheng, 1998; Bao and Koch, 1999). For the purposes of this study, the oxygen fractionation factor equation Eq. (4) defined by Yapp (1990a) will be used for both goethite and hematite because it has been found to be consistent with several other studies (Girard et al., 2000; Poage et al., 2000; Yapp, 2001; Sjostrom et al., 2004). The following equation describes the relationship between temperature and the goethite–water oxygen isotope fractionation factor:

$$1000\ \ln {}^{18}\alpha = \frac{1.63 \times 10^{6}}{T^{2}} - 12.3 \quad \text{(Yapp, 1990a)}. \tag{4}$$

Using Eq. (1) and the methods highlighted above, the vast majority of the goethite samples yield a calculated temperature of formation between 20 and 25 °C, with a mean calculated temperature of 22 ± 2 °C (Table. 1; Fig. 4). This estimated temperature is in agreement with the modern mean annual temperature range for the Barberton region, at 20–22 °C. One outlier falls well out of this temperature range, with a calculated temperature of formation of 1 °C. This sample has the lowest δD value ($\delta D = -146‰$) and one of the heaviest $\delta^{18}O$ values ($\delta^{18}O = 1.0‰$). If this goethite formed from meteoric water at 22 °C, it would be expected to have a $\delta^{18}O$ of −2.0‰. It is possible the disproportionately heavy oxygen value may result from quartz contamination, which would have the affect of producing a heavy $\delta^{18}O$ value while the δD would remain unaffected. However, the $\delta^{18}O$ of quartz in the ironstone pods range from 12.4‰ to 18.2‰ (de Ronde et al., 1994). This sample would have to contain 10–15% quartz with this range of isotopic compositions to shift the measured $\delta^{18}O$ value from the expected value of −2.0‰ to

the observed value of 1‰. This degree of contamination is not evidenced in the XRD spectrum or microprobe analysis and suggests quartz contamination is not responsible for the oxygen value observed here. Given the low SiO_2 content of goethites, potential quartz contamination is not expected to alter $\delta^{18}O$ values by more than 0.35–0.5‰ in all but the single most contaminated sample and in most cases is within the 0.3‰ error of the oxygen isotope measurement. As a result, calculated temperatures for goethite are most consistent with formation from near surface waters not hydrothermal systems or hot (55–85 °C) Archean ocean waters (Knauth and Lowe, 2003).

In addition to the calculated temperatures of formation, hydrogen isotopes further support formation from modern meteoric waters rather than Archean ocean water. The range of δD values of goethite observed here (δD = −125‰ to −146‰) is lower than the δD value of a goethite in equilibrium with the Archean ocean, which would be approximately −111‰. This calculation is based on the assumption that the δD of the Archean ocean was no lighter than δD ∼ −18‰, which is supported by mass-balance estimates of hydrogen loss through time and stable isotope analyses of ancient marine rocks (Sheppard and Epstein, 1970; Harper et al., 1988; Yui et al., 1990; Lécuyer et al., 1996, 1998). Instead, the goethite values are more consistent with formation from modern meteoric waters for this area and elevation that have an estimated mean annual δD value of ∼−24‰ (Bowen and Wilkinson, 2002), and would form goethite with a δD value of ∼−117‰.

This analysis underscores the utility of using combined hydrogen and oxygen isotopes of goethite to determine conditions of formation. Oxygen isotope analyses alone give ambiguous results. On the basis of oxygen isotope analyses alone, the $\delta^{18}O$ from the Barberton ironstone pods (−0.7‰ to 1.0‰) could indicate an ancient origin. These $\delta^{18}O$ values are consistent with formation from a hot (∼60–65 °C) Archean ocean (estimated to be between 55 and 85 °C by Knauth and Lowe, 2003) with a $\delta^{18}O$ value of −1‰ (Shackleton, 1967). Taken together however, oxygen and hydrogen isotope analyses of goethite from the ironstone pods strongly suggest that goethite formed in surface or shallow subsurface spring systems from recent meteoric waters. All but one goethite sample plot parallel to the Global Meteoric Water Line along a 20–25 °C isotherm (Fig. 4). This result is important because it is unlikely that post crystallization hydrogen exchange would produce δD values that pair with unexchanged oxygen to produce an array parallel to the Meteoric Water Line. These data suggest goethite formation: (1) over a narrow range of temperatures of 20–25 °C that are similar to the modern mean annual temperature of 20–22 °C for the Mendon Farm, Barberton area; and (2) from isotopically light meteoric waters with a $\delta^{18}O$ of ∼−5‰, which is similar to the calculated mean annual $\delta^{18}O$ values (−4.6‰) for modern precipitation for the Mendon Farm, Barberton region (Bowen and Wilkinson, 2002).

It could be argued that goethite is a modern weathering product of Archean-age hematite within the ironstone pods. Unfortunately, oxygen isotope analyses of hematite cannot discriminate between an Archean hydrothermal or modern meteoric origin. In the case of hematite from the ironstone pods, the calculated oxygen isotope value of waters of formation could range from ∼−1‰ for the Archean ocean, to −3‰ to −6‰ for modern meteoric waters for the Barberton region (Bowen and Wilkinson, 2002), and depend upon the assumed temperature of formation of hematite. If hematite formed at temperatures of 90–110 °C, like those near a hydrothermal vent, its $\delta^{18}O$ values are consistent with formation from an Archean ocean, which in the absence of ice sheets, may have a $\delta^{18}O$ value of approximately −1‰ (Shackleton, 1967). If hematite formed at temperatures between 40 and 55 °C, which is consistent with the interpretation of Lowe and Byerly (2003) that hematite in ironstone pods formed in subaerial warm springs, then they would be in equilibrium with modern meteoric waters with a $\delta^{18}O \sim -5‰$ (Bowen and Wilkinson, 2002), and similar to the calculated $\delta^{18}O$ of water in equilibrium with measured goethites.

In light of the uncertainty provided by oxygen isotope analyses of hematite alone, we provide REE data that, in our view, demonstrates that both hematite and goethite from the ironstone pods are derived from recent remobilization of iron and REE in subaerial spring systems from surrounding rock units.

5.2. REE systematics of goethite and hematite

Our understanding of the Archean ocean, in part, is based upon REE patterns of preserved Archean sediments. These REE patterns reflect hydrothermal inputs to the early ocean (Derry and Jacobsen, 1990; Danielson et al., 1992; Gao and Wedepohl, 1995; Bau and Dulski, 1999), chemical stratification of marine waters (German et al., 1991; Möller and Bau, 1993; Schijf et al., 1994; Kuhn et al., 1998), the rise of an oxidizing atmosphere (Fryer, 1977; Towe, 1991), as well as later chemical weathering and diagenetic effects. As such, we examined REE patterns in goethite and hematite from the ironstone pods in the Fig Tree and Onverwacht groups, Barberton greenstone belt, as well as a suite of eleven locally associated silicified ultramafic rocks, black cherts, felsic tuff, sideritic ironstone, and chert/sandstone, to address the origin of ironstone-forming solutions. The REE patterns of goethite and hematite from the ironstone pods are consistent with formation in shallow subaerial spring systems from iron-rich solutions resulting from the weathering of local bedrock, rather than Archean, hydrothermal vent structures. This conclusion is based upon the following observations.

First, positive Eu anomalies for hematite and goethite, a common marker for high-temperature hydrothermal inputs in ocean precipitates, average ∼1.7, which is similar to that of subjacent bedrock, and lower than expected for Archean iron oxyhydroxides formed directly at hydrothermal vents.

The abundance of Eu relative to other REEs in iron oxyhydroxides provides a measure of the relative influence of high-temperature hydrothermal fluids and marine waters. At low temperatures, Eu exists in the Eu^{3+} state; however in hot, reducing solutions typical of oceanic hydrothermal plumes (>250 °C), Eu exists primarily in the Eu^{2+} state. High-temperature hydrothermal alteration of primary minerals discriminates against divalent Eu resulting in highly Eu-enriched fluids (Sverjensky, 1984). While modern seawater does not display any enrichment of Eu relative to shale abundances (Elderfield and Greaves, 1982), fluids emanating from mid-ocean ridges, black smokers, and closely associated chemical precipitates show significant Eu enrichment, with Eu anomalies in fluids typically between Eu/Eu* = 6.3–19.7 (Michard and Albarède, 1986) and as high as Eu/Eu* = 72.9 (Derry and Jacobsen, 1990; Edmonds and German, 2004). Because of the high Eu concentrations in hydrothermal fluids, the relative shale-normalized abundance of Eu in Archean BIFs and other chemical sediments has been used to address the degree of hydrothermal inputs to the ocean and show that Fe-rich Archean water was characterized by a positive Eu anomaly (Dymek and Klein, 1988; Derry and Jacobsen, 1990; Danielson et al., 1992; Möller and Bau, 1993; Bau and Dulski, 1996). Hematite and goethite samples from the ironstone pods, however, have only slightly positive shale-normalized Eu anomalies, with hematite having an average Eu/Eu*of 1.7 and goethite an average Eu/Eu* of 1.6 (Table 2). These values are lower than expected for chemical precipitates believed to be forming in direct contact with hydrothermal vent fluids and comparable or slightly less than the measured Eu/Eu* for associated ferruginous sediments and silicified ultramafic rocks.

Second, hematite and goethite fall along a mixing line between the measured shale-normalized $HREE_{Avg}/LREE_{Avg}$ and Eu/Eu* of locally associated Archean felsic volcanic rocks and silicified ultramafic rocks, suggesting that the REE within these oxides are derived from post-depositional weathering of local bedrock units. To test whether the goethite and hematite formed as a result of recent weathering of bedrock or hydrothermal activity in the Archean we examined the $HREE_{Avg}/LREE_{Avg}$ (defined as the ratio of the average shale-normalized HREE value, including Gd, Tb, Dy, Ho, Er, Tm, Yb, and Lu and the average shale-normalized LREE value, including La, Pr, Nd, and Sm) and Eu/Eu* systematics of iron oxides and a suite of adjacent bedrock types. Although oxidative scavenging of REEs in the relatively oxygen-rich conditions of the modern ocean may result in non-conservative REE mixing behavior between ocean waters and hydrothermal solutions (Bau and Dulski, 1999), chemical precipitates forming at and around hydrothermal vent structures in the chemically stratified or low-oxygen conditions of the Archean ocean (Drever, 1974; Derry and Jacobsen, 1990) should record a REE distribution of some mixture of hydrothermal and marine waters. Precipitates formed in this fashion should fall on a mixing line between the chemical composition of hydrothermal vents that have strong positive Eu anomalies and no or relatively low HREE enrichment (Mitra et al., 1994; Douville et al., 1998; Bau and Dulski, 1999) and normal marine waters which display a general HREE enrichment and no Eu anomaly (Elderfield and Greaves, 1982; Sholkovitz et al., 1999). On a plot of Eu/Eu* versus $HREE_{Avg}/LREE_{Avg}$, this conservative mixing line between purely hydrothermal and purely marine fluids has a steep negative slope where even dilute hydrothermal–marine mixtures can be distinguished from strictly marine waters (Fig. 9). Because of the strong enrichment of Eu in deep-ocean hydrothermal solutions, fluids comprised of only 1% hydrothermal solutions and 99% ocean water will still display Eu/Eu* values of approximately 9, and $HREE_{Avg}/LREE_{Avg}$ of nearly 2.5, and can be clearly distinguished from modern seawater, which has Eu/Eu* values of 1.1 and $HREE_{Avg}/LREE_{Avg}$ of nearly 3.4. As a result, iron-oxides formed in association with deep-marine Archean hydrothermal systems should display REE evidence of the addition of a hydrothermal component, even with only very small additions of hydrothermal solutions.

In contrast, hematite and goethite from the ironstone pods fall along a mixing line between local Archean felsic volcanic rocks and silicified ultramafic rocks (Fig. 9). The Eu/Eu* and $HREE_{Avg}/LREE_{Avg}$ values of hematite and goethite are intermediate between the end member values of ferruginous strata and silicified ultramafic rocks (Eu/Eu* = 2.1; $HREE_{Avg}/LREE_{Avg} \sim 3.4$) and felsic vol-

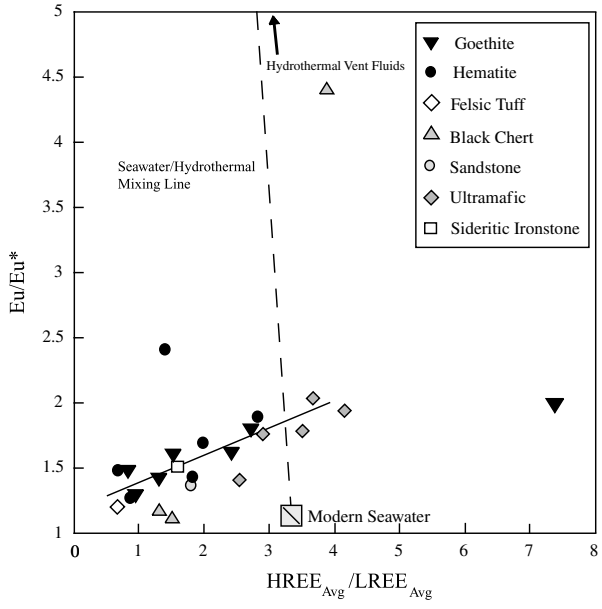

Fig. 9. Mixing-model for goethite and hematite samples from the ironstone pods. A plot of the $HREE_{Avg}/LREE_{Avg}$ (HREE defined as the average shale-normalized value of Gd, Tb, Dy, Ho, Er, Tm, Yb, and Lu; LREE defined as the average shale-normalized value of La, Pr, Nd, and Sm) versus the Eu/Eu* value shows the degree of mixing between bulk ocean water and hydrothermal vent fluids. A mixing line shows the hypothetical coordinates of solutions with varying degrees of hydrothermal and marine inputs. Hematites and goethites from the Barberton ironstone pods fall along a mixing line between silicified ultramafic rocks and local felsic volcanoclastic sands.

canic rocks ($Eu/Eu^* = 1.2$; $HREE_{Avg}/LREE_{Avg} = 0.7$), and plot closely to associated sandstone and sideritic ironstones. Since no significant fractionation of Eu from other trivalent REEs is expected to occur during chemical weathering processes and formation of secondary minerals (Sverjensky, 1984), the position of hematite and goethites along this mixing line suggests varying degrees of REE input from different locally associated bedrock. In total, these data suggest that the REE in the goethite and hematite samples are derived primarily from weathering of the sideritic ironstones and cherts, ferruginous strata, and ultramafic and felsic volcanic rocks and do not reflect an Archean hydrothermal origin.

Third, the presence of variable Ce anomalies in goethite and hematite components of the ironstone pods provides evidence of post-depositional terrestrial weathering processes involving oxidative scavenging of Ce on hematite and precipitation of goethite from an evolved near-surface fluid. Several hematites have a positive Ce anomaly ($Ce/Ce^* = 1.3–3.4$) and several goethites have a negative Ce anomaly ($Ce/Ce^* = 0.2–0.5$) which contrasts with REE patterns for locally associated Archean units that have slightly negative or no Ce anomalies (Table 2). Hematites and goethites formed in the Archean ocean in a near-hydrothermal vent environment should lack a Ce anomaly since, in the absence of an oxygen-rich environment, Ce^{3+} oxidation to relatively insoluble Ce^{4+} will not readily occur, and Ce will fractionate similar to the trivalent REE. This has been shown to be the case in the 3.2–3.3 Ga near-hydrothermal vent iron oxide deposits at Pilbara, Australia, which lack a significant Ce anomaly (Kato et al., 1998). While several of the hematite and goethite samples from the Barberton ironstone pods similarly show no anomalous Ce, this in itself does not provide any indication of the age or mode of depositional processes. However, the presence of variable Ce anomalies in several of the iron oxide samples strongly suggests mobilization and oxidation of iron- and REE-bearing solutions after the initial deposition of stratigraphically associated cherts, ultramafic units, and felsic volcanic rocks. We prefer an explanation that involves oxidative scavenging of Ce on the surface of iron oxides from REE-rich solutions derived from the chemical weathering of local bedrock units.

In general, abiotic Ce oxidation at the Earth's surface proceeds at a slow rate. However, the surface of iron oxyhydroxides catalyze the oxidation of the dissolved Ce^{3+} form to the less soluble Ce^{4+} phase at the low pH ($pH < 5$) conditions of oxide precipitation (Bau, 1994, 1999) resulting in Ce precipitation and the generation of positive Ce anomalies in iron oxyhydroxides. If the Ce in hematite is derived from the weathering of local sideritic ironstones and ultramafic and felsic volcanic rocks and the resultant oxidation of REE and iron-bearing solutions, the positive Ce anomaly seen in some hematite, and the overall enrichment of Ce in hematite relative to goethites and stratigraphically associated units, may be generated by (1) initial precipitation of hematite, followed by (2) continued growth of hematite where at the surface of the growing hematite, Ce^{3+} oxidizes to Ce^{4+}, becoming relatively insoluble and remaining with oxide precipitates (Bau, 1999). The negative Ce anomaly observed in goethite could result from oxide precipitation from solutions in which oxidative scavenging of Ce on hematite has already occurred, resulting in iron-rich solutions that are depleted in Ce with respect to other REE. Goethite precipitation may also be expected to be accompanied by an increase in the pH of solutions, relative to hematite formation, because iron and manganese oxides display greater sorption of REE at higher pH (Koeppenkastrop and De Carlo, 1992; Bau et al., 1998; Bau, 1999). As a result, iron oxides precipitated from Ce depleted solutions at higher pH will be expected to display negative Ce anomalies and general REE enrichment over oxides precipitated at lower pH (Koeppenkastrop and De Carlo, 1992; Bau et al., 1998; Bau, 1999), which is consistent with the REE distribution observed in Barberton iron oxides.

6. Conclusion

In light of the significance of Archean ironstone bodies as possible geochemical proxies for the chemical composition of the ancient ocean, it is important to distinguish ancient sediments from relatively recent formations. The combined stable isotope and Rare Earth Element approach used here provides a valuable technique for analyzing iron-oxide bodies of questionable age. Specifically, stable isotope and REE data for hematite and goethite from ironstone pods resting on the rocks of the Fig Tree and Onverwacht Groups on Mendon Farm in the Barberton greenstone belt, show that these large iron-rich bodies are relatively recent, shallow, subaerial spring deposits derived from the remobilization of iron and REE in surrounding host rock.

The oxygen and hydrogen isotope and REE data for hematite and goethite are consistent with the interpretations of Lowe and Byerly (2003) that the Barberton ironstone pods formed through deposition from modern surface and shallow subsurface spring waters which derived their iron through leaching of surrounding iron-rich Archean units. The present results are consistent with the following paragenesis: (1) migration of modern meteoric-derived, acidic, warm (40–55 °C) solutions through surrounding Archean sideritic sedimentary layers resulting in Fe dissolution; (2) precipitation of hematite from ascending iron and REE-bearing fluids in the shallow subsurface; and (3) precipitation of goethite in the shallow subsurface and as surface spring deposits as a result of further iron oxidation and pH change at ambient surface temperatures of ~20–25 °C.

Acknowledgments

We thank Guangchao Li for assistance with ICP measurements and Robert Jones for assistance with electron microprobe analyses. We thank Dennis Bird for many helpful discussions. This manuscript benefited from thoughtful reviews and suggestions by Crayton J. Yapp,

Michael Bau, and Andrey Bekker. This work was supported by NASA Exobiology Program Grants NCC-2-721, NAG5-98421, and NNG04GM43G to D.R.L.

Associate editor: James Farquhar

References

Alibert, C., McCulloch, M.T., 1993. Rare-Earth Element and neodymium isotopic compositions of the banded iron-formations and associated shales from Hamersley, Western-Australia. *Geochim. Cosmochim. Acta* **57**, 187–204.

Bao, H.M., Koch, P.L., 1999. Oxygen isotope fractionation in ferric oxide-water systems: low temperature synthesis. *Geochim. Cosmochim. Acta* **63**, 599–613.

Bao, H.M., Koch, P.L., 2000. Oxygen isotopic composition of ferric oxides from recent soil, hydrologic, and marine environments. *Geochim. Cosmochim. Acta* **64**, 2221–2231.

Bau, M., 1994. Modeling of Rare-Earth Element partitioning between particles and solution in aquatic environments—comment. *Geochim. Cosmochim. Acta* **58**, 4521–4523.

Bau, M., Dulski, P., 1996. Distribution of yttrium and Rare-Earth Elements in the Penge and Kuruman iron-formations, Transvaal Supergroup, South Africa. *Precamb. Res.* **79**, 37–55.

Bau, M., Usui, A., Pracejus, B., Mita, N., Kanai, Y., Irber, W., Dulski, P., 1998. Geochemistry of low-temperature water-rock interaction: evidence from natural waters, andesite, and iron-oxyhydroxide precipitates at Nishiki-numa iron-spring, Hokkaido, Japan. *Chem. Geol.* **151**, 293–307.

Bau, M., 1999. Scavenging of dissolved yttrium and rare earths by precipitating iron oxyhydroxide: experimental evidence for Ce oxidation, Y–Ho fractionation, and lanthanide tetrad effect. *Geochim. Cosmochim. Acta* **63**, 67–77.

Bau, M., Dulski, P., 1999. Comparing yttrium and rare earths in hydrothermal fluids from the Mid-Atlantic Ridge: implications for Y and REE behaviour during near-vent mixing and for the Y/Ho ratio of Proterozoic seawater. *Chem. Geol.* **155**, 77–90.

Becker, R.H., Clayton, R.N., 1976. Oxygen isotope study of a Precambrian banded iron-formation, Hamersley range, Western-Australia. *Geochim. Cosmochim. Acta* **40**, 1153–1165.

Bjerrum, C.J., Canfield, D.E., 2002. Ocean productivity before about 1.9 Gyr ago limited by phosphorus adsorption onto iron oxides. *Nature* **417**, 159–162.

Bolhar, R., Kamber, B.S., Moorbath, S., Fredo, C.M., Whitehouse, M.J., 2004. Characterization of early Archean chemical sediments by trace element signatures. *Earth Planet. Sci. Lett.* **222**, 43–60.

Bowen, G.J., Wilkinson, B., 2002. Spatial distribution of delta O-18 in meteoric precipitation. *Geology* **30**, 315–318.

Channer, D.M.D., de Ronde, C.E.J., Spooner, E.T.C., 1997. The Cl^-–Br^-–I^- composition of ~3.23 Ga modified seawater: implications for the geological evolution of ocean halide chemistry. *Earth Planet. Sci. Lett.* **150**, 325–335.

Clayton, R.N., Mayeda, T.K., 1963. The use of bromine pentafluoride in the extraction of oxygen from oxides and silicates for isotopic analysis. *Geochim. Cosmochim. Acta* **27**, 43–52.

Craig, H., 1961. Isotopic variations in meteoric waters. *Science* **133**, 1702–1703.

Danielson, A., Möller, P., Dulski, P., 1992. The europium anomalies in banded iron formations and the thermal history of the oceanic-crust. *Chem. Geol.* **97**, 89–100.

Dansgaard, W., 1964. Stable isotopes in precipitation. *Tellus* **16**, 436–542.

de Ronde, C.E.J., de Wit, M.J., Spooner, E.T.C., 1994. Early Archean (greater than 3.2 Ga) Fe-oxide rich, hydrothermal discharge vents in the Barberton greenstone-belt, South-Africa. *GSA Bull.* **106**, 86–104.

de Ronde, C.E.J., Ebbesen, T.W., 1996. 3.2 by of organic compound formation near sea-floor hot springs. *Geology* **24**, 791–794.

de Ronde, C.E.J., Channer, D.M.D., Faure, K., Bray, C.J., Spooner, E.T.C., 1997. Fluid chemistry of Archean sea-floor hydrothermal vents: implications for the composition of circa 3.2 Ga seawater. *Geochim. Cosmochim. Acta* **61**, 4025–4042.

de Wit, M.J., Hart, R., Martin, A., Abbott, P., 1982. Archean abiogenic and probable biogenic structures associated with mineralized hydrothermal vent systems and regional metasomatism, with implications for greenstone belt studies. *Econ. Geol.* **77**, 1783–1802.

Derry, L.A., Jacobsen, S.B., 1990. The chemical evolution of Precambrian seawater—evidence from REEs in banded iron formations. *Geochim. Cosmochim. Acta* **54**, 2965–2977.

Douville, E., Bienvenu, P., Charlou, J.L., Donval, J.P., Fouquet, Y., Appriou, P., Gamo, T., 1998. Yttrium and rare earth elements in fluids from various deep-sea hydrothermal systems. *Geochim. Cosmochim. Acta* **63**, 627–643.

Drever, J.I., 1974. Geochemical model for origin of Precambrian banded iron formations. *GSA Bull.* **85**, 1099–1106.

Dymek, R.F., Klein, C., 1988. Chemistry, petrology and origin of banded iron-formation lithologies from the 3800-Ma Isua Supracrustal Belt, West Greenland. *Precamb. Res.* **39**, 247–302.

Edmonds, H.N., German, C.R., 2004. Particle geochemistry in the Rainbow hydrothermal plume, Mid-Atlantic Ridge. *Geochim. Cosmochim. Acta* **68**, 759–772.

Elderfield, H., Greaves, M.J., 1982. The Rare-Earth Elements in seawater. *Nature* **296**, 214–219.

Fryer, B.J., 1977. Rare-Earth evidence in iron-formations for changing Precambrian oxidation-states. *Geochim. Cosmochim. Acta* **41**, 361–367.

Gao, S., Wedepohl, K.H., 1995. The negative Eu anomaly in Archean sedimentary rocks—implications for decomposition, age and importance of their granitic sources. *Earth Planet. Sci. Lett.* **133**, 81–94.

German, C.R., Holliday, B.P., Elderfield, H., 1991. Redox cycling of Rare-Earth Elements in the suboxic zone of the Black-Sea. *Geochim. Cosmochim. Acta* **55**, 3553–3558.

Girard, J.P., Razanadranorosoa, D., Freyssinet, P., 1997. Laser oxygen isotope analysis of weathering goethite from the lateritic profile of Yaou, French Guiana: Paleoweathering and paleoclimatic implications. *Appl. Geochem.* **12**, 163–174.

Girard, J.P., Freyssinet, P., Chazot, G., 2000. Unraveling climatic changes from intraprofile variation in oxygen and hydrogen isotopic composition of goethite and kaolinite in laterites: an integrated study from Yaou, French Guiana. *Geochim. Cosmochim. Acta* **64**, 409–426.

Girard, J.P., Freyssinet, P., Morillon, A.C., 2002. Oxygen isotope study of Cayenne duricrust paleosurfaces: implications for past climate and laterization processes over French Guiana. *Chem. Geol.* **191**, 329–343.

Harper, G.D., Bowman, J.R., Kuhns, R., 1988. A field, chemical, and stable isotope study of subseafloor metamorphism of the Josephine Ophiolite, California-Oregon. *J. Geophys. Res.* **93**, 4625–4656.

Harrison, C.G.A., 1999. Constraints on ocean volume change since the Archean. *Geophys. Res. Lett.* **26**, 1913–1916.

Hein, J.R., Yeh, H.W., Gunn, S.H., Gibbs, A.E., Chung-Ho, W., 1994. Composition and origin of hydrothermal ironstones from Central Pacific seamounts. *Geochim. Cosmochim. Acta* **58**, 179–189.

Hoefs, J., Muller, G., Schuster, K.A., 1987. The Fe–Mn ore-deposits of Urucum, Brazil—an oxygen isotope study. *Chem. Geol.* **65**, 311–319.

Jackson, M.L., Chin, H.L., Zelazny, L., 1982. Oxides, hydroxides, and aluminosilicates. In: Klute, A. (Ed.), *Methods of Soil Analysis Part I: Physical and Mineralogical Methods*. American Society of Agronomy, Soil Science Society of America, Madison, WI, pp. 101–150.

Kämpf, N., Schwertmann, U., 1982. The 5 M NaOH concentration treatment for iron-oxides in soils. *Clays Clay Min.* **30**, 401–408.

Kasting, J.F., 1987. Theoretical constraints on oxygen and carbon-dioxide concentrations in the Precambrian Atmosphere. *Precamb. Res.* **34**, 205–229.

Kato, Y., Ohta, I., Tsunematsu, T., Watanabe, Y., Isozaki, Y., Maruyama, S., Imai, N., 1998. Rare earth element variations in mid-Archean banded iron formations: Implications for the chemistry of ocean and

continent and plate tectonics. *Geochim. Cosmochim. Acta* **62**, 3475–3497.

Knauth, P., Lowe, D.R., 2003. High Archean climatic temperature inferred from oxygen isotope geochemistry of cherts in the 3.5 Ga Swaziland Supergroup, South Africa. *GSA Bull.* **115**, 566–580.

Koeppenkastrop, D., De Carlo, E.H., 1992. Sorption of Rare-Earth Elements from seawater onto synthetic mineral particles—an experimental approach. *Chem. Geol.* **95**, 251–263.

Kuhn, T., Bau, M., Blum, N., Halbach, P., 1998. Origin of negative Ce anomalies in mixed hydrothermal–hydrogenetic Fe–Mn crusts from the Central Indian Ridge. *Earth Planet. Sci. Lett.* **163**, 207–220.

Lécuyer, C., Gruau, G., Früh-Green, G.L., Picard, C., 1996. Hydrogen isotope composition of Early Proterozoic seawater. *Geology* **24**, 291–294.

Lécuyer, C., Gillet, P., Robert, F., 1998. The hydrogen isotope composition of seawater and the global water cycle. *Chem. Geol.* **145**, 249–261.

Lowe, D.R., Byerly, G.R., 1999. Stratigraphy of the west-central part of the Barberton greenstone belt, South Africa: geologic evolution of the Barberton greenstone belt, South Africa. *Geol. Soc. Am. Special Paper* **329**, 1–36.

Lowe, D.R., Byerly, G.R., 2003. Ironstone pods in the Archean Barberton greenstone belt, South Africa: Earth's oldest seafloor hydrothermal vents reinterpreted as Quaternary subaerial springs. *Geology* **31**, 909–912.

Michard, A., Albarède, F., 1986. The REE content of some hydrothermal fluids. *Chem. Geol.* **55**, 51–60.

Mitra, A., Elderfield, H., Greaves, M.J., 1994. Rare-Earth Elements in submarine hydrothermal fluids and plumes from the Mid-Atlantic Ridge. *Mar. Chem.* **46**, 217–235.

McLennon, S.M., 1989. Rare Earth Elements in sedimentary rocks: influence of provenance and sedimentary processes. *Rev. Mineral.* **21**, 169–200.

Möller, P., Bau, M., 1993. Rare-Earth patterns with positive cerium anomaly in alkaline waters from Lake Van, Turkey. *Earth Planet. Sci. Lett.* **117**, 671–676.

Perry, E.C., Tan, F.C., Morey, G.B., 1973. Geology and stable isotope geochemistry of Biwabik iron formation, Northern Minnesota. *Econ. Geol.* **68**, 1110–11125.

Perry, E.C., Ahmad, S.N., 1983. Oxygen isotope geochemistry of Proterozoic chemical sediments. *Geol. Soc. Am. Memoirs* **161**, 253–263.

Poage, P.A., Sjostrom, D.J., Goldberg, J., Chamberlain, C.P., Furniss, G., 2000. Isotopic evidence for Holocene climate change in the northern Rockies from a goethite-rich ferricrete chronosequence. *Chem. Geol.* **166**, 327–340.

Rozanski, K., Araguas-Araguas, L., Gonfiantini, R., 1993. Isotopic patterns in modern global precipitation. In: Swart, P.K., Lohmann, K.C., McKenzie, J.A., Savin, S. (Eds.), *Climate Change in Continental Isotopic Records, Geophysical Monograph 78*. American Geophysical Union, Washington, DC, pp. 1–36.

Sharp, Z.D., Atudorei, V., Durakiewicz, T., 2001. A rapid method for determination of hydrogen and oxygen isotope ratios from water and hydrous minerals. *Chem. Geol.* **178**, 197–210.

Sheppard, S.M., Epstein, S., 1970. D/H and O-18/O-16 ratios of minerals of possible mantle or lower crustal origin. *Earth Planet. Sci. Lett.* **9**, 232–242.

Schijf, J., Debaar, H.J.W., Millero, F.J., 1994. Kinetics of Ce and Nd scavenging in Black-Sea waters. *Mar. Chem.* **46**, 345–359.

Shackleton, N., 1967. Oxygen isotope analyses and Pleistocene temperatures re-assessed. *Nature* **215**, 15–17.

Sholkovitz, E.R., Elderfield, H., Szymczak, R., Casey, K., 1999. Island weathering: river sources of rare earth elements to the Western Pacific Ocean. *Mar. Chem.* **68**, 39–57.

Sjostrom, D.J., Hren, M.T., Chamberlain, C.P., 2004. Oxygen isotope records of goethite from ferricrete deposits indicate regionally varying Holocene climate change in the Rocky Mountain region, USA. *Quat. Res.* **61**, 64–71.

Sverjensky, D.A., 1984. Europium redox equilibria in aqueous-solution. *Earth Planet. Sci. Lett.* **67**, 70–78.

Taylor, S.R., McLellan, S.M., 1985. *The Continental Crust: Its Composition and Evolution*. Blackwell, Oxford.

Towe, K.M., 1991. Aerobic carbon cycling and cerium oxidation—significance for Archean oxygen levels and banded iron-formation deposition. *Palaeogeog. Palaeoclim. Palaeoecol.* **97**, 113–123.

Yapp, C.J., Pedley, M.D., 1985. Stable hydrogen isotopes in iron-oxides. II. D/H variations among natural goethites. *Geochim. Cosmochim. Acta* **49**, 487–495.

Yapp, C.J., 1987. Oxygen and hydrogen isotope variations among goethites (Alpha-FeOOH) and the determination of paleotemperatures. *Geochim. Cosmochim. Acta* **51**, 355–364.

Yapp, C.J., 1990a. Oxygen isotopes in iron oxides. 1. Mineral-water fractionation factors. *Chem. Geol.* **85**, 329–335.

Yapp, C.J., 1990b. Oxygen isotopes in iron oxides. 2. Possible constraints on the depositional environment of a Precambrian quartz–hematite banded iron formation. *Geochim. Cosmochim. Acta* **85**, 337–344.

Yapp, C.J., 1991. Oxygen isotopes in an oolitic ironstone and the determination of goethite delta-O-18 values by selective dissolution of impurities—the 5 M NaOH method. *Geochim. Cosmochim. Acta* **55**, 2627–2634.

Yapp, C.J., 1993. Paleoenvironment and the oxygen-isotope geochemistry of ironstone of the Upper Ordovician Neda Formation, Wisconsin, USA. *Geochim. Cosmochim. Acta* **57**, 2319–2327.

Yapp, C.J., 1997. An assessment of isotopic equilibrium in goethites from a bog iron deposit and a lateritic regolith. *Chem. Geol.* **135**, 159–171.

Yapp, C.J., 1998. Paleoenvironmental interpretations of oxygen isotope ratios in oolitic ironstones. *Geochim. Cosmochim. Acta* **62**, 2409–2420.

Yapp, C.J., 2000. Climatic implications of surface domains in arrays of δD and delta O-18 from hydroxyl minerals: goethite as an example. *Geochim. Cosmochim. Acta* **64**, 2009–2025.

Yapp, C.J., 2001. Rusty relics of earth history: iron(III) oxides, isotopes, and surficial environments. *Annu. Rev. Earth Planet. Sci.* **29**, 165–199.

Yui, T.F., Yeh, H.W., Lee, C.W., 1990. A stable isotope study of serpentinization in the Fengtien Ophiolite, Taiwan. *Geochim. Cosmochim. Acta* **54**, 1417–1426.

Zheng, Y.F., 1998. Oxygen isotope fractionation between hydroxide minerals and water. *Phys. Chem. Min.* **25**, 213–221.